

Feasibility theory reconciles alternative approaches to neuromuscular control

Brian A. Cohn^{a,1}, May Szedlák^{b,1}, Bernd Gärtner^b, and Francisco J. Valero-Cuevas^{c,d}

^aUniversity of Southern California, Department of Computer Science, Los Angeles, CA, USA; ^bETH Zurich, Department of Theoretical Computer Science, Zurich, Switzerland; ^cUniversity of Southern California, Department of Biomedical Engineering, Los Angeles, CA, USA; ^dUniversity of Southern California, Division of Biokinesiology and Physical Therapy, Los Angeles, CA, USA

This manuscript was compiled on August 20, 2017

We present a conceptual and computational framework to unify today's theories of neuromuscular control called feasibility theory. We begin by describing how the musculoskeletal anatomy of the limb, the need to control individual tendons, and the physics of a motor task uniquely specify the family of all valid muscle activations that accomplish it (its 'feasible activation space'). For our example of static force production with a finger with seven muscles, computational geometry characterizes, in a complete way, the structure of feasible activation spaces as 3-dimensional polytopes embedded in 7-D. The feasible activation space for a given task is the landscape where all neuromuscular learning, control, and performance must occur. This approach unifies current theories of neuromuscular control because the structure of feasible activation spaces can be separately approximated as either low-dimensional basis functions (synergies), high-dimensional joint probability distributions (Bayesian priors), or fitness landscapes (to optimize cost functions).

Neuromechanics | Motor Control | Tendon actuation | ...

This PNAS journal template is provided to help you write your work in the correct journal format. Instructions for use are provided below.

How the nervous system selects specific levels of muscle activations (i.e. a muscle activation pattern) for a given motor task continues to be hotly debated. Some suggest the nervous system either combines low-dimensional synergies (1–7), learns probabilistic representations of valid muscle activation patterns (8–11), or optimizes physiologically-tenable cost functions (12–17). At the core of this problem lies the nature of 'feasible activation spaces,' and the computational challenge of describing and understanding their high-dimensional structure (for an overview, see (18)). A feasible activation space is the family of valid solutions (i.e. muscle activation patterns) available to the nervous system to produce a given motor task. Fig. 1 illustrates the neuromechanical interactions that define the feasible activation space for a particular task.

The most the nervous system can do, therefore, is select a specific muscle activation pattern from within the feasible activation space—as muscle activation patterns outside of this space are, by definition, inappropriate for the task. In fact, the feasible activation space defines the landscape upon which all neuromuscular learning and performance must occur. Understanding neuromuscular control is, therefore, equivalent to understanding how the nervous system finds, explores, inhabits, and exploits the structure of feasible activation spaces (1–6, 22).

But the 'curse of dimensionality' (23–25) makes it computationally challenging to calculate, describe, and understand the nature and structure of high-dimensional feasible activation spaces (4, 12, 19, 20, 26–28)—even for an isolated human fin-

ger or cat leg generating everyday static forces (1, 18, 29, 30). This is due to the computational complexity of algorithms applied upon high dimensional spaces.

Current theories of neuromuscular control are alternative responses to the curse of dimensionality, which at times can be seen as competing, rather than complementary. However, the fundamental neuromechanics of the limb and the physics of the task are the common ground for all theories. Thus, understanding the nature and structure of feasible activation spaces would help compare, contrast and combine these alternative approaches to neuromuscular control.

We now propose a conceptual and computational framework to provide complete characterizations of feasible activation spaces, thereby contextualizing and unifying multiple theories of neuromuscular control. As an example, we leverage prior work (1, 21, 31) to now describe the structure of the feasible activation space for the seven muscles of the index finger when producing static fingertip force. This is the type of fingertip force observed when, for example, pressing hard on a table without finger movement, and is also referred to as an isometric force task. In this case, the feasible activation space is a polytope embedded in 7-dimensional muscle activation space. A polytope is the name given to bounded convex polyhedra in dimensions higher than 3. Our computational approach hinges on the efficient sampling and complete representation of the structure of high-dimensional polytopes. This then characterizes all valid muscle activation patterns. These computational techniques can scale up to ~40 dimensions, which suffices to analyze the neural control of all muscles in a extant vertebrate limb systems. By providing a complete characterization of all muscle activation patterns for a given motor task, we are able

Significance Statement

Wings take flight, eyes refract light, and muscles manipulate bones within the interplaying constraints of Newtonian physics. Here we apply the basic tenets of physics to the field of neuromechanical control, to elucidate the neuro-physical-motor landscape upon which evolution and learning operate. With three interweaving hypotheses of motor control in the literature, we fill the gap between the disparate approaches by recontextualizing the problem of force control as a physical constraints problem, thereby lighting the stage of optimal, synergistic, and bayesian control.

Please provide details of author contributions here.

Please declare any conflict of interest here.

¹A.O.(Author One) and A.T. (Author Two) contributed equally to this work (remove if not applicable).

²To whom correspondence should be addressed. E-mail: author.two@email.com

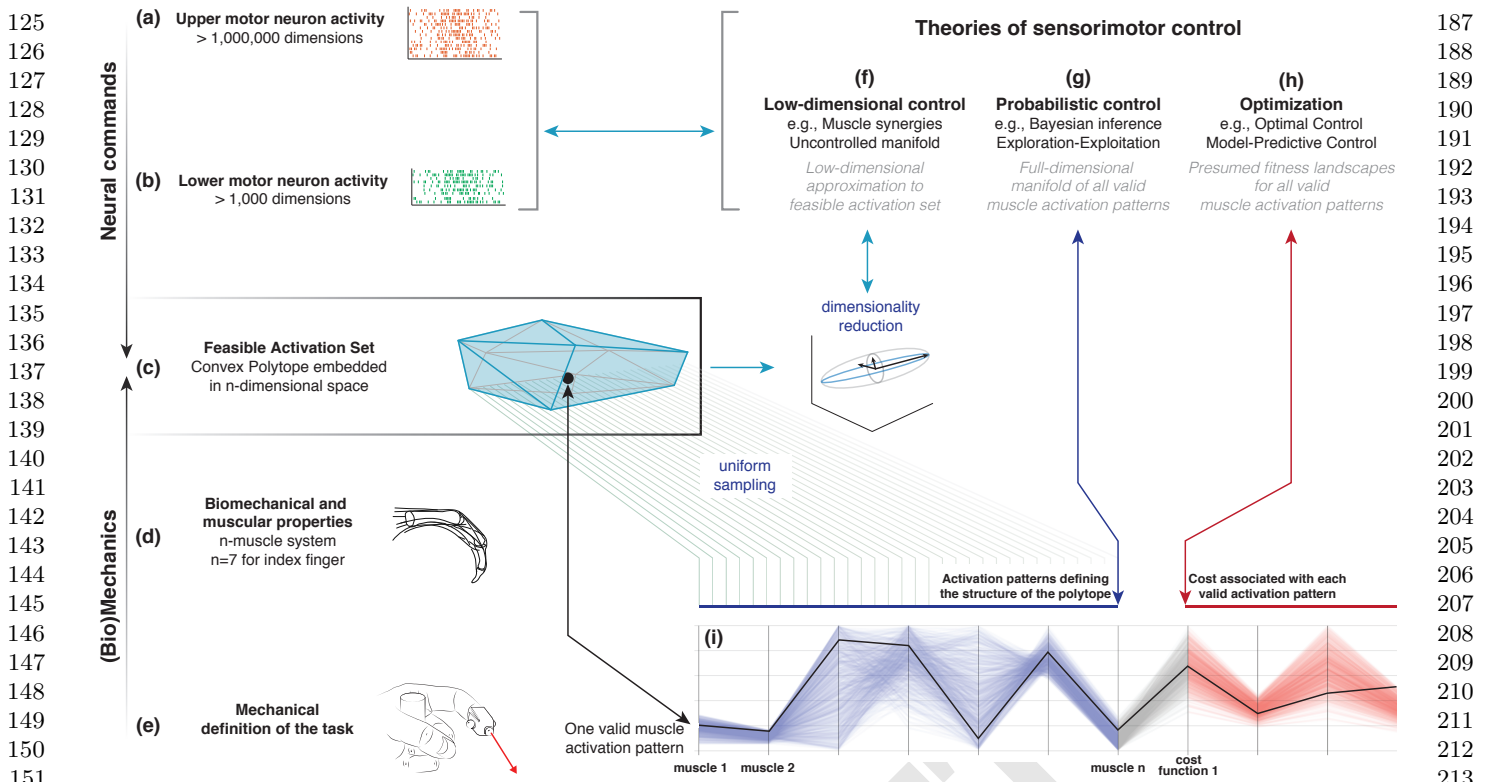


Fig. 1. Feasible activation spaces guiding sensorimotor control of a task. The descending motor command for a given task is issued by the primary motor cortex (a), which projects onto *alpha*-motor neuron pools in the spinal cord (b). The combined drive to all *alpha*-motor neurons of a muscle can be considered its total muscle activation level (a value between 0 and 1). If we consider that motor commands are sent to multiple independently controlled muscles, then the overall motor command can be conceptualized as a multi-dimensional *muscle activation pattern* (i.e., a point) in a high-dimensional *muscle activation space* (12, 19–21) (c). For that muscle activation pattern to be valid, it has to elicit muscle forces (d) capable of satisfying the mechanical requirements of the task—in this case a well directed fingertip force (e). Given the large number of muscles in vertebrates, there is muscle redundancy; there is a large number of valid muscle activation patterns that can produce a given task. We propose that our novel ability to characterize the high-dimensional structure of feasible activation spaces (i) allows us to compare, contrast and reconcile today's three dominant approaches to redundancy in sensorimotor control (f, g, h).

to compare, contrast, combine—and reconcile—today's three dominant approaches to neuromuscular control.

Results

The goal of this work is to use different perspectives to describe the high-dimensional structure of these feasible activation spaces; we then show how these spaces allow us to unify today's theories of neuromuscular control. We used our realistic index finger model to calculate the feasible activation space for the task of producing static fingertip force in the distal direction (see Fig. 1). The model represents each muscle's contribution to fingertip force as a directed force vector at the fingertip; there are 7 of these force vectors at the index fingertip. As described briefly in the Methods, Hit-and-Run is a method in polytope sampling that we use to sample from the infinite number of muscle activations within the feasible activation space. In effect, given a fingertip task force and the maximum linear fingertip forces each muscle creates, we can collect the muscle activations required to produce that task. As we can now collect thousands of muscle activation patterns for any isometric force task, we examined how the feasible activation spaces (and their representations) change with increasing task intensity in the distal direction (Fig. 1e).

We collected points for multiple task intensities between 0% (i.e., pure co-contraction without output force) and 100%

of maximal static force.

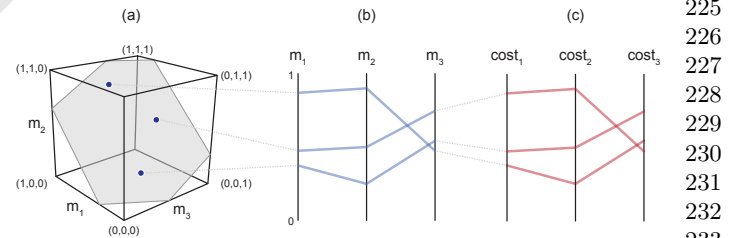
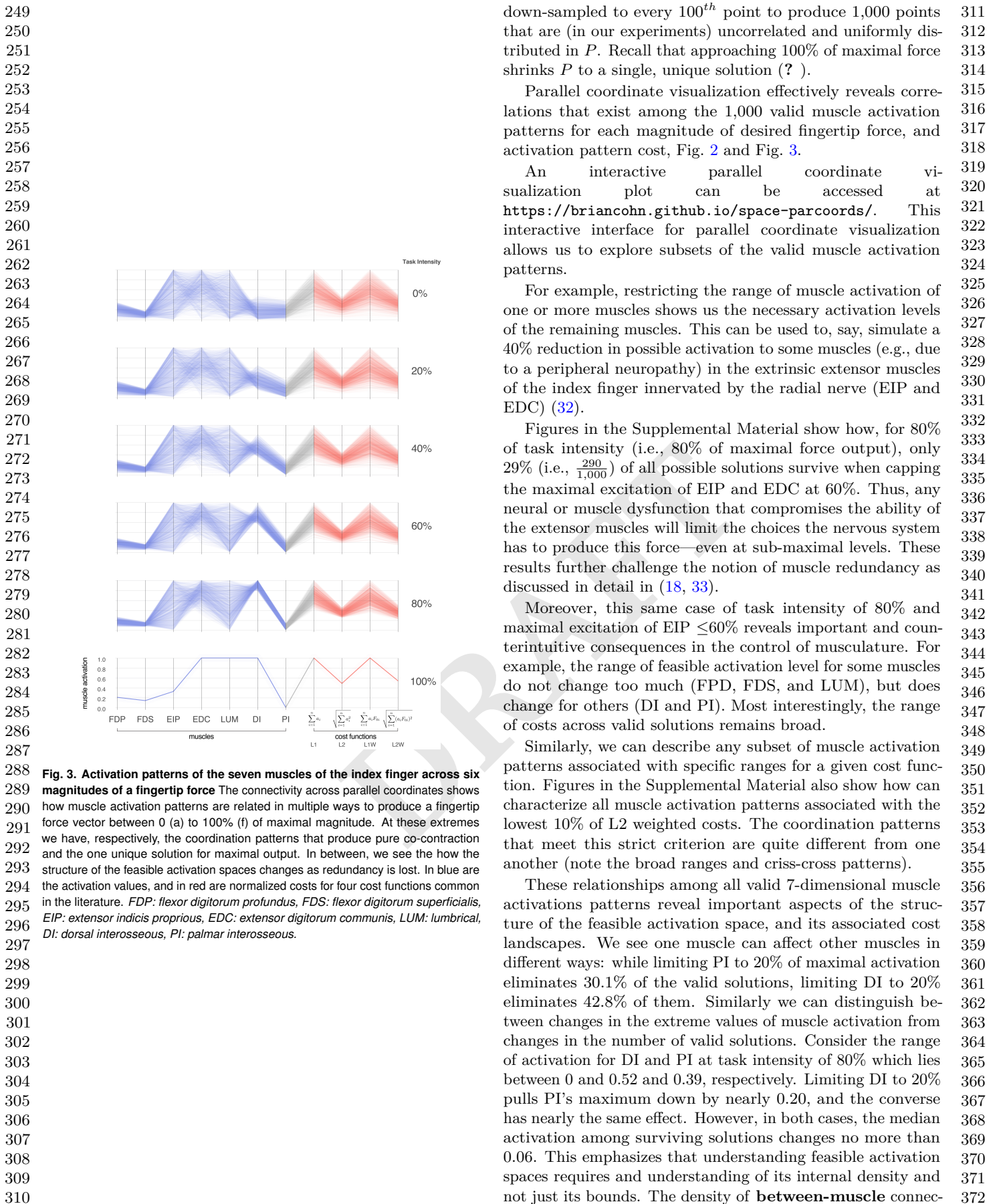


Fig. 2. Characterizing the high-dimensional structure of a feasible activation space via parallel coordinates. Consider three points (i.e., muscle activation patterns in Supplemental Fig. ??e) from the feasible activation space (a). The activation level for each muscle (i.e., the coordinates of each point) are sewn across three vertical parallel axes (b). As is common when evaluating multiple valid coordination patterns, each point can be assigned a cost as per an assumed *cost function*. The associated cost for each muscle activation pattern can also be shown as an additional dimension. We show three representative cost functions (c). Activation levels are bound between 0 and 1, and costs are normalized to their respective observed ranges.

Parallel coordinate visualization naturally reveals the structure of the feasible activation space. We used Hit-and-Run to sample from feasible activation spaces for 6 task intensities, labeled as task intensities α of 0.0, 0.2, 0.4, 0.6, 0.8 and 1.0. For each task intensity, we ran 100,000 Hit-and-Run iterations and



373 tivity is seen directly by the density of the lines connecting
 374 the different muscles and cost functions. The **within-muscle**
 375 density can be computed by binning points at each activation
 376 level value. 435
 436
 437
 438
 439
 440
 441
 442
 443
 444
 445
 446
 447
 448

377 Lastly, those same connecting lines in the parallel coordinate
 378 visualization allow us to characterize the interrelatedness
 379 of valid solutions in 7-dimensional space. For example, the
 380 lines connecting FDP and FDS are mostly parallel, indicating
 381 a strong positive correlation. In fact, looking at these lines
 382 allows one to directly see and understand the Pearson product-
 383 moment correlation coefficients of 0.99, -0.50, and -0.06 in the
 384 adjacent muscle pairs FDP—FDS, LUM—DI, and EIP—EDC,
 385 respectively. The interactive parallel coordinate visualization
 386 also allows for any pairwise comparison by simply dragging
 387 and reordering the vertical axes—and hovering over individual
 388 data rows highlight an individual valid activation pattern atop
 389 all others. 449
 450
 451
 452
 453
 454
 455
 456
 457
 458
 459

390 **Low-dimensional approximations to the feasible activation
 391 space.** We applied PCA (Principal Component Analysis) to
 392 the valid muscle activation patterns sampled uniformly at
 393 random from the feasible activation space. We show results for
 394 10 levels of task intensity. However, we did this in an iterative
 395 fashion to replicate the fact that experimental studies can only
 396 collect a finite amount of data from each subjects. Thus, from
 397 the total pool of 10,000 sub-sampled points sampled by Hit-
 398 and-Run (i.e., accepting every 100th point from 100,000 total
 399 samples to remove potential autocorrelation among points);
 400 sample sizes of 10, 100, and 1,000 points (i.e., simulated ‘ex-
 401 perimental’ sample sizes) were replicated 100 times each. We
 402 applied PCA to each set of sampled points. 460
 461
 462
 463
 464
 465
 466
 467
 468
 469
 470
 471
 472
 473
 474
 475
 476
 477
 478
 479
 480
 481
 482
 483
 484
 485
 486
 487

403 The variance explained by PC1 and PC2 (and its boxplot
 404 distribution) for all iterations are shown to change with task
 405 intensity for all sample sizes (Fig. 5). Explaining about 13–15%
 406 of the variance, PC3 is exactly equal to the remaining variance
 407 not explained by the first two components—this is a result of
 408 the feasible activation space being a 3-dimensional polytope
 409 P by construction (i.e., recall that 4 task constraints applied
 410 to 7 muscles produce a 3-dimensional polytope embedded in
 411 the 7-dimensional muscle activation space). 470
 471
 472
 473
 474
 475
 476
 477
 478
 479
 480
 481
 482
 483
 484
 485
 486
 487

413 The boxplots in Fig. 5 quantify how different amounts of
 414 data change the estimates of variance explained by PC1 and
 415 PC2 with task intensity (c.f. labels a vs. b vs. c). We see
 416 this dispersion is small in the center and right columns. Note
 417 that the ratio of variance explained between PC1 and PC2
 418 between 50 to 80% of task intensity is indicative of changes in
 419 the aspect ratio of the feasible activation space—which we see
 420 changes with task intensity. 488
 489
 490
 491
 492
 493
 494
 495
 496

421 Importantly, using experimentally realistic samples sizes of
 422 10 repetitions per subject (leftmost column) not only does not
 423 capture this change, but its standard deviation is large enough
 424 to blur the statistically significant differences that are known
 425 to appear with larger (but experimentally unrealistic) sample
 426 sizes. The impact of impoverishing the number of samples fed
 427 to PCA reminds us that inadequate amounts of data obfuscate
 428 the underlying changes in the structure of the data analyzed
 429 (Fig. 5). 489
 490
 491
 492
 493
 494
 495
 496

430 There were also important changes in the loadings of the
 431 PC1 and PC2 vectors. While the ratio of variance explained
 432 between PC1 and PC2 gives a sense of the aspect ratio of
 433 the feasible activation space, the loadings of PC1 and PC2
 434 speak to its orientation. Fig. 6 shows how the loadings of
 435
 436
 437
 438
 439
 440
 441
 442
 443
 444
 445
 446
 447
 448
 449
 450
 451
 452
 453
 454
 455
 456
 457
 458
 459
 460
 461
 462
 463
 464
 465
 466
 467
 468
 469
 470
 471
 472
 473
 474
 475
 476
 477
 478
 479
 480
 481
 482
 483
 484
 485
 486
 487

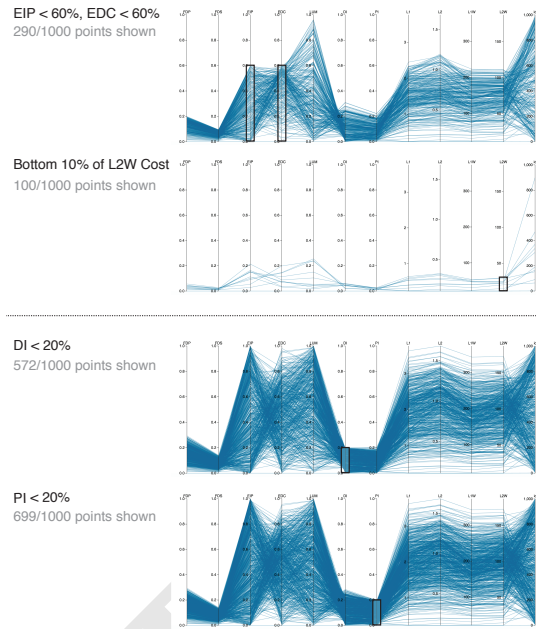


Fig. 4. Supplemental Figure: Posthoc constraints on a task intensity of 80%
 Here we show four unique examples of constraints applied to the points collected from the feasible activation space. With this, we can rapidly predict how index finger control must change in the event of weakness in specific muscles. We also can see how many points remain once the constraints are added—signaling how the structure of the feasible force space is affected.

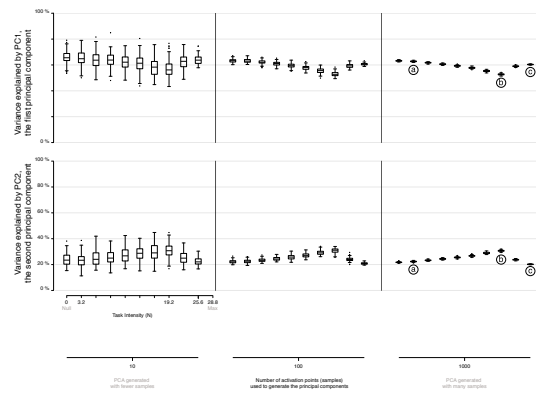
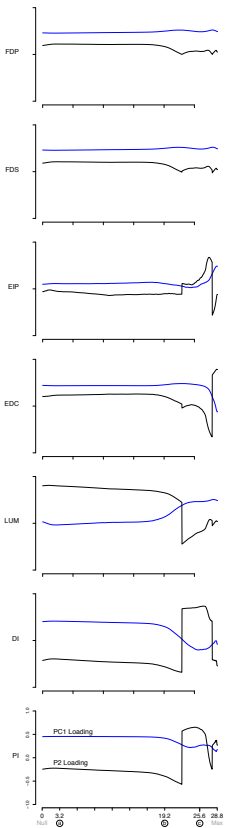


Fig. 5. Approximating the structure of feasible activation spaces via principal components analysis (PCA) is sensitive to both the number of points used and the intensity of the task. Rows show the variance explained by the first (top) and second (bottom) principal components with increasing data points (left to right). It is not possible to generalize the variance explained across tasks intensities, and large numbers of points (*i.e.*, > 100) are needed to confidently estimate the real changes in variance explained as a function of task intensity (cf. points labeled a, b, c).

497 the PC1 and PC2 vectors change across labels a, b, and c
498 (Fig. 5) corresponding to 11, 66 and 88% of task intensity,
499 respectively. What these loadings indicate are the direction in
500 7-dimensional space, which changes dramatically.

501 These changes we see in (i) the lower and upper bounds of
502 activations, and in (ii) the relative variance explained and (iii)
503 loadings for PC1 and PC2, demonstrate that the size, shape
504 and orientation of the feasible activation space changes with
505 task intensity. Moreover, these changes represent the best-case
506 scenario given the absence of experimental noise, within- and
507 across-subject variability, and measurement error.



539 **Fig. 6. PCA loadings change dramatically as task intensity increases** For each
540 of 1,000 task intensities, we collected 1,000 points from the feasible activation space,
541 and computed three principal components. Note that the signs of the loadings depend
542 on the numerics of the PCA algorithm, and are subject to arbitrary flips in sign—
543 thus for clarity we plot them such that FDP's loadings in PC1 are positive at all
544 task intensities. Synergies at representative task intensities a, b, c in Fig. 5 differ.
545 This reflects changes in the geometric structure of the feasible activation space as
546 redundancy is lost.

547 **Changes in the probabilistic structure of the feasible activation space with increasing task intensity, or how muscle redundancy is lost.** The maximal static fingertip force vector in
548 a given direction is produced by a single and unique combination
549 of muscle activations. In contrast, any sub-maximal mag-
550 nitude of that same vector is produced by an infinite number
551 of solutions (12, 18, 19, 34). Our analysis of feasible activation
552 spaces at different task intensities allows us to characterize how
553 this redundancy changes and is lost. The histogram heatmaps
554 in Fig. 7 illustrate the changes and shrinking of within-muscle
555 density of valid activation levels for sub-maximal forces, con-

556 verging to a single solution for maximal force output. These
557 surface plots show how the normalized histograms (of 1,000
558 valid activation levels for each muscle) change at each of 100
559 levels of task intensity between 0 and 1. Following a muscle's
560 column from bottom to top shows the activation histograms
561 for each magnitude of distal force and ending, naturally, with
562 a spike about the unique value at maximal force production.

563 The flat areas in each surface plot (e.g. clearly visible
564 for DI) represent muscle activation levels that are not valid
565 for that task intensity. That is, there exist no valid muscle
566 activation patterns that contain that muscle at that level, and
567 thus no points are found there.

568 These plots show the nature and rate of convergence to the
569 unique solution for maximal force output across muscles. We
570 find that the histograms of activation levels for each muscle
571 need not be symmetric, nor have the same shape (skewness
572 and kurtosis) as the magnitude of the output force increases.
573 For some muscles the convergence accelerates after 60% or
574 80% of task intensity (as in LUM and EIP), while others
575 converge monotonically along the entire progression (e.g. DI
576 and PI). The peaks (i.e. modes) of each histogram at each
577 task intensity represents the slice of the polytope that has
578 the largest relative volume along that muscle dimension (i.e.,
579 greatest frequency of that level of muscle activation across all
580 valid solutions). Importantly, for most muscles (FDP, FDS,
581 EIP, EDC, and LUM), the mode is not necessarily located at
582 the same relative level of activation needed for maximal force
583 output. That is, the histogram at high levels of force is not
584 simply a shifted version of the histogram at low levels of force.
585 The histograms for DI are the exception, whose modes seems
586 to scale linearly with task intensity.

587 These histograms, in conjunction with the results in the
588 parallel coordinate visualization, also demonstrate that the
589 structure of feasible activation spaces cannot be inferred from
590 their bounding boxes alone (i.e., upper and lower activation
591 bounds for each muscle). An immediate example is how,
592 for most task intensities, both EIP and LUM have similar
593 lower and upper bounds near 0 and 1, respectively—yet their
594 distributions are thoroughly distinct.

Discussion

595 **Summary.** Feasibility theory, as a conceptual and computa-
596 tional approach, is a means to pierce the curse of dimensionality
597 to establish a physics-based ground truth for neuromuscular
598 control. This practical approach can now characterize—in a
599 complete way—the set of all valid ways to activate multiple
600 muscles to produce a given task. Feasible activation spaces are,
601 in fact, the neuromechanical landscapes upon which all
602 neuromuscular learning, control, and performance must occur.
603 Therefore, we provide an integrative and unifying perspective
604 that demonstrates how today's dominant theories of neuromuscular
605 control are alternative approximations to feasible activation
606 spaces from optimization, geometric, and probabilistic
607 perspectives.

608 **The value of a cost function.** Optimization is the oldest com-
609 putational approach to finding valid muscle activation patterns
610 that produce limb function (e.g., (12)). While optimization is
611 a reasonable hypotheses to explore neuromuscular control (15),
612 some criticize it as mathematical abstraction that anthropo-
613 morphizes neurons with the ability to choose, evaluate and
614

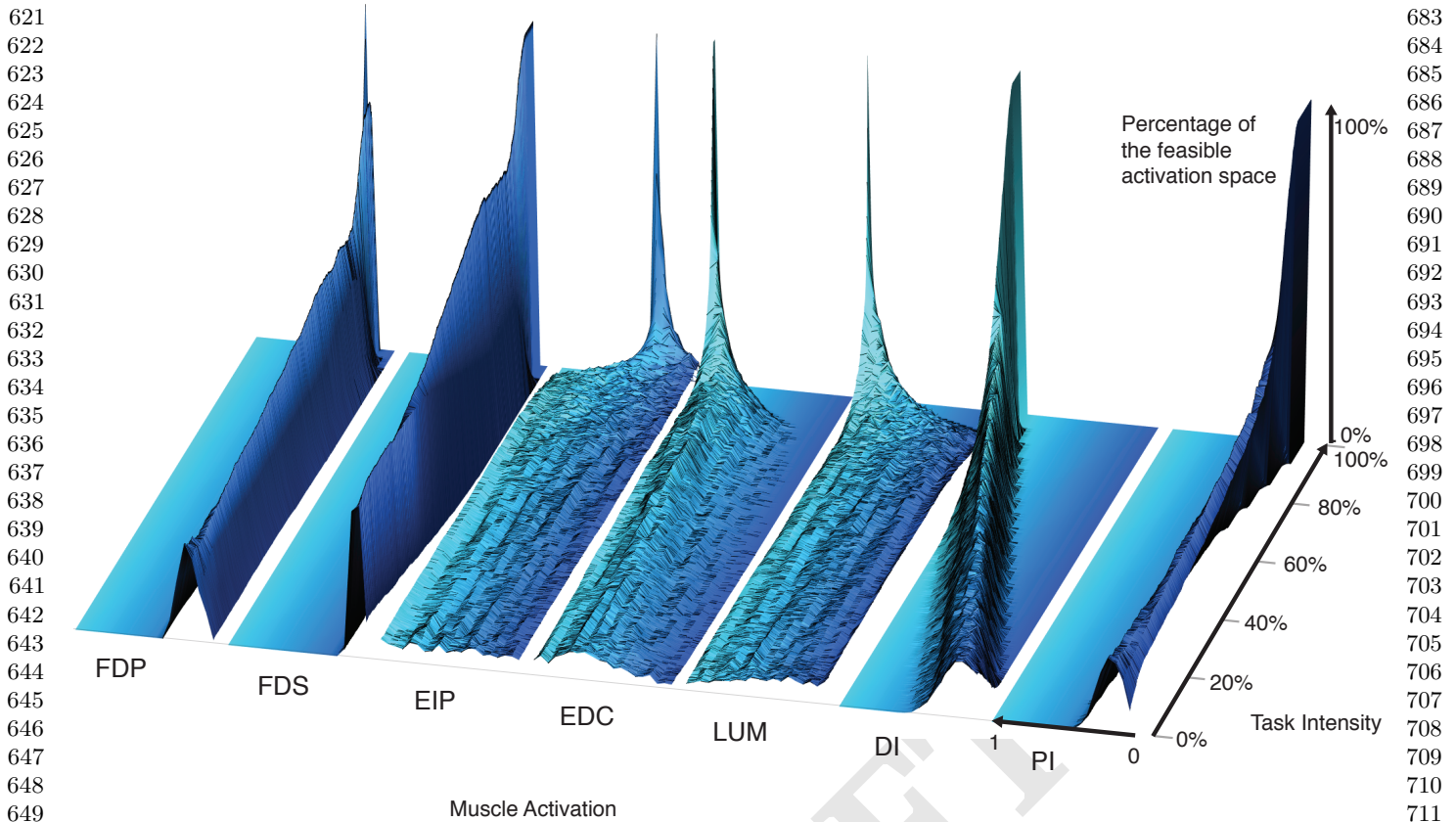


Fig. 7. The within-muscle probabilistic structure of feasible muscle patterns across 1,000 levels of fingertip task intensity. The changes in the breadth and height for each muscle reveal muscle-specific consequences of task intensity on their probability distributions. The cross-section of each density plot is the 50-bin histogram of activation for each muscle, at that task intensity. Height represents the percentage of solutions for that task. The axis going into the page indicates increasing fingertip task intensity up to 100% of maximal. Color is used to provide perspective.

follow cost functions in high-dimensions (35, 36). There is an intimate relationship between optimization and feasible activation spaces (37). Optimization is analogous to finding a best solution in the dark—guided by repeated evaluations of a cost-function. Computing the feasible activation space is then a means to ‘turn on the lights’ to see all possible valid solutions independently of cost (18). Our complete sampling of high-dimensional feasible activation spaces (38, 39) allows us to compare and contrast *families* of solutions instead of *individual* optimal solutions for a particular cost function. Fig. 3 demonstrates a complete description of families of valid coordination patterns and their relationship to alternative costs. Importantly, similar valid muscle activation patterns can have dissimilar costs, and vice versa.

Because these explorations can be done for alternative cost functions, they can provide quantitative overall descriptions of high-dimensional ‘cost landscapes.’ By not having to insist on (or settle for) individual optimal—or near-optimal—solutions, we now have the same ability the nervous system has to explore, compare and contrast multiple valid ways to coordinate muscles. Importantly, the relationships among valid muscle activation patterns emerge naturally from the physical properties of the limb and definition of the task. This cost-agnostic approach allows us to re-evaluate our assumptions about what the nervous system cares—and does not care—about. Lastly, this cost-agnostic approach also provides a powerful tool for

inverse optimization, i.e., uncovering latent cost functions from data (40). Our comparison across cost functions using parallel coordinates is already a form of inverse optimization.

Structure, correlation, and synergies. The physical properties of the limb and definition of the task also define a low-dimensional structure of the feasible activation space (18). Therefore, it is expected that experimental recordings of muscle activations during limb function will exhibit a dimensionality that is smaller than the number of muscles (1, 7). Thus, applying PCA to the points sampled from the feasible activation space also finds that few PCs can explain the variance in the data.

This application of PCA at increasing task intensities (i.e., as muscle redundancy is lost) allows us to demonstrate—for the first time to our knowledge—several important features and limitations of dimensionality reduction. For example, we see that the aspect ratio (Fig. 5) and orientation (Fig. 6) of the feasible activation spaces change as their size shrinks (Fig. 7). Thus, such *descriptive* synergies extracted from limited experimental observations likely do not generalize well across task intensities. It is important to distinguish *descriptive* synergies (the dominant approach in the literature to extract synergies from experimental data using dimensionality reduction techniques such as PCA) from *prescriptive* synergies (those known to be implemented by the controller) (18).

This also has important consequences to motor control and

745 learning. Producing force vectors at the endpoint of a finger
746 or limb with accurate magnitude and direction are critical
747 for versatile manipulation and locomotion (41–43). If a given
748 synergy can produce such accurate force vectors only for a
749 given task intensity (and thus inaccurate ones at other in-
750 tensities), then the attractiveness of synergies to simplify the
751 neuromuscular control of the limb is reduced. To compensate,
752 the nervous system would need to learn, recall and implement
753 specific synergies for each force level. In prior experimental
754 work, we have shown that the nervous system produces accu-
755 rate fingertip forces of different magnitudes by, instead, likely
756 scaling a remembered muscle activation pattern to produce
757 forces of different magnitudes, together with a full-dimensional,
758 real-time error correction neural controller (44). Note that
759 interpreting this experimental result still as a synergy-based
760 approach would defeat the purpose of synergies as a means to
761 simplify the control by reducing its dimensionality.

762 Our results also show how experiments with realistically
763 moderate numbers of participants and test trials likely do
764 not contain sufficient data to produce robust estimates of de-
765 scriptive synergies across task intensities. As per the curse
766 of dimensionality, sampling uniformly at random from high-
767 dimensional spaces is exponentially difficult. Thus, even for
768 this anatomically complete 7-muscle finger model, PCA de-
769 pends strongly on the number of independent observations,
770 such as uncorrelated trials from one subject or different sub-
771 jects. Figure 5 shows that 100 to 1,000 such ideal data points
772 from a simulated ‘test subject’ are needed to produce accurate
773 estimates of changes in PC1 and PC2 with task intensity (c.f.
774 labels a vs. b vs. c). Future studies should explore how many
775 experimental data points are sufficient from a given subject
776 when recording from only a subset of the many (20+) muscles
777 of human limbs in the presence of experimental noise, inherent
778 stochasticity of EMG, and within- and between-subject vari-
779 ability. Some studies have begun to ask subjects to explore
780 different ways to perform a given task (45) (i.e., estimate
781 the structure of the feasible activation space), but in practice
782 such studies cannot likely collect sufficient data uniformly
783 at random to obtain accurate estimates of the descriptive
784 synergies (1). While our results suggest caution when inter-
785 preting synergies obtained experimentally, we underscore that
786 dimensionality-reduction is a useful approach to capture global
787 geometric properties of feasible activation spaces.

788

789 **Toward probabilistic neuromuscular control.** Our results are
790 particularly empowering for the emerging field of probabilistic
791 neuromuscular control (8? –10). Suppose that the nervous
792 system uses some form of probabilistic or Bayesian learning
793 and control strategy. Such approach requires two enabling—
794 and biologically feasible—elements: *trial-and-error iterative*
795 *exploration*, and *memory-based exploitation* of the probability
796 density functions used to approximate the feasible activation
797 spaces (8). The parallel coordinate plots and histograms
798 in Fig. 2 and 7 provide, to our knowledge, the first com-
799 plete (38, 39) characterization of such multi-dimensional joint
800 probability density functions for a realistic tendon-driven sys-
801 tem performing a well-defined task.

802 These techniques and results now empower the study of
803 fundamental aspects of probabilistic control. For example, an
804 organism can only execute so many trial-and-error iterations
805 during learning, likely too few to completely and exhaustively
806 sample the high-dimensional feasible space of interest. This

807 makes it much more likely that, by virtue of being more
808 easily found, an organism will find and preferentially exploit
809 the strong modes (i.e., narrow and high peaks in Figs. 3, 4,
810 and 7) of the multi-dimensional probability density functions
811 than any other region of feasible activation spaces. Thus,
812 first, the maximal ranges of feasible activations described by
813 the bounding box (29, 30) may have little practical bearing
814 on how those tasks are learned and executed. And second,
815 those same strong modes would represent strong attractors
816 to create and reinforce motor habits. Habitual control has
817 been proposed based on experimental and empirical data as an
818 alternative to a strict optimization approach to neuromuscular
819 control (35). Our work now provides the computational means
820 to link habitual to probabilistic control. This allows us to
821 generate testable hypotheses of how these motor habits are
822 defined by the structure of the feasible activation space, how
823 they are learned by the organism, and how difficult or easy it
824 is to break out of them.

825 Thus, motor learning likely needs to proceed from adopting
826 easily-found solutions independently of their cost, to using
827 some low dimensional approximation to the gradient of the cost
828 landscape, to then transitioning to less likely but potentially
829 less costly subregions of the solutions space. This integrative
830 perspective leads us to propose a hybrid approach to motor
831 learning and execution where the practical limits on trial-and-
832 error iterations are coupled with the low-dimensional structure
833 of the solution space to enable some form of heuristic local
834 optimization to create sub-optimal motor habits. Importantly,
835 the organism performs strict optimization or synergy control at
836 its peril. Take, for example, the case of a 2-dimensional feasible
837 activation space embedded in 3-D, Fig. ??e. Taking a step from
838 any one valid point to another valid point on the plane runs the
839 risk of ‘falling off’ the solution space and failing at the task—a
840 risk that is exponentially exacerbated in higher-dimensions.
841 Thus, improvements in the neighborhood of a good solution
842 necessarily risk task failure and potential injury. These are all
843 arguments in support of the evolutionary and developmentally
844 useful strategy to use good-enough control based on habit or
845 sensorimotor memory rather than optimization (35, 46). This
846 may explain why mass practice and coaches are so critical to
847 achieve elite athletic performance (47).

848

849

850

851

852 **Clinical implications.** This line of thinking has consequences
853 to neurorehabilitation. Neurological conditions disrupt feasi-
854 ble activation spaces, be it by affecting anatomy of the limb,
855 muscle strength and independence with which muscles can be
856 controlled. Functional recovery following the disruption, if
857 not destruction, of the landscape of valid muscle activation
858 patterns requires re-learning existent, or building new, proba-
859 bility density functions. This occurs just when older adults
860 suffer from reduced perceptuo-motor learning rates (48).

861 A probabilistic landscape for neuromuscular function begins
862 to explain why neurorehabilitation in aging adults is so difficult
863 (e.g., (49)) and why motor learning in children takes thousands
864 of repetitions (50)—while also generating new rehabilitation
865 strategies, and testable hypotheses around them, that leverage
866 knowledge of the nature and structure of feasible activation
867 spaces.

<p>869 Materials and Methods</p> <p>870 The methods to obtain feasible activation spaces for ‘tendon-driven’</p> <p>871 limbs are described in detail in the textbook <i>Fundamentals of</i></p> <p>872 <i>Neuromechanics</i> and references therein (18). This tendon-driven</p> <p>873 approach explicitly and distinctly avoids the conceptual approach</p> <p>874 to combine multiple muscle actions into net torques at each joint.</p> <p>875 Rather, it emphasizes studying the individual actions of all mus-</p> <p>876 cles at all levels of analysis, from their neural activation to their</p> <p>877 contributions to fingertip force. We describe them briefly here.</p> <p>878</p> <p>Theory. Consider a tendon-driven limb, such as a finger, with n</p> <p>879 independently controllable muscles, where we define the neural</p> <p>880 command to each muscle as a positive value of activation between</p> <p>881 0 (no activation) and 1 (maximal activation). We can then vi-</p> <p>882 sualize the set of all feasible neural commands (i.e., all possible</p> <p>883 muscle activation patterns) as the points contained in a positive</p> <p>884 n-dimensional cube with sides of length equal to 1. A specific muscle</p> <p>885 activation pattern is a <i>point</i> (i.e., an n-dimensional vector \mathbf{a}) in this</p> <p>886 n-dimensional cube (12, 19–21). Now consider a specific task, such</p> <p>887 as producing a vector of static force with the fingertip, as when</p> <p>888 holding an object. Clearly, not all muscle activation patterns inside</p> <p>889 the n-dimensional cube can produce that desired static fingertip</p> <p>890 force vector: bone lengths, kinematic degrees of freedom, anatomical</p> <p>891 routing, posture, and muscle strength inequities define the subset</p> <p>892 of points in the n-cube that can produce a fingertip force vector of a</p> <p>893 specific magnitude and direction. As described in (12, 18–20) the</p> <p>894 musculoskeletal anatomy of the limb, the need to control individ-</p> <p>895 ual tendons, and the physics of a motor task uniquely specify a</p> <p>896 polytope embedded in \mathbb{R}^n (i.e., the feasible activation space). This</p> <p>897 polytope contains the family of (potentially infinite) valid muscle</p> <p>898 activation patterns that can produce this static force production</p> <p>899 task. However, these valid muscle coordination patterns are not ar-</p> <p>900 bitrarily different because, by construction, the geometric structure</p> <p>901 of the polytope that contains them defines strict spatial correlations</p> <p>902 among them (1).</p> <p>903</p> <p>System of linear equations to simulate static force production by a</p> <p>tendon-driven system Consider producing a vector of static force</p> <p>904 with the endpoint of the limb in a given posture. The constraints</p> <p>905 that define that task (i.e., the direction and magnitude of the force</p> <p>906 vector at the endpoint) are linear equations (18) that come from the</p> <p>907 mapping between neural activation of individual muscles to static</p> <p>908 endpoint forces and torques the limb can produce. This mapping is</p> <p>909 linearly modeled by the equation</p> <p>910</p> $\begin{pmatrix} f_x \\ f_y \\ f_z \\ \tau_x \\ \tau_y \\ \tau_z \end{pmatrix} = \mathbf{w} = H\mathbf{a} = H \begin{pmatrix} a_1 \\ a_2 \\ a_3 \\ \dots \\ a_n \end{pmatrix}, \mathbf{a} \in [0, 1]^n \quad [1]$ <p>911 where H is the matrix of linear constraints defined by the muscu-</p> <p>912 loskeletal anatomy of the limb (29), \mathbf{a} is the input vector of n muscle</p> <p>913 activations, $\mathbf{f} \in \mathbb{R}^m$ is the m-dimensional limb output ‘wrench’ (i.e.,</p> <p>914 the forces and torques the finger can produce at the endpoint).</p> <p>915 The output wrench, m, is at most 6-dimensional (i.e., 3 forces</p> <p>916 and 3 torques) depending on the number of kinematic degrees of</p> <p>917 freedom of the limb, and usually $m < n$ because limbs have more</p> <p>918 muscles than kinematic degrees of freedom (18). Muscles can only</p> <p>919 pull, so elements of \mathbf{a} cannot be negative, and are capped at 1 (i.e.,</p> <p>100% of maximal muscle activation).</p> <p>920 What are the muscle coordination patterns that produce a given</p> <p>921 task? As explained in (18), the task of producing a static fingertip</p> <p>922 force vector is defined by specifying the desired values for the</p> <p>923 elements of the endpoint forces and torques of \mathbf{w}. Each such</p> <p>924 constraint equation defines a hyperplane of dimension $n-1$, and their</p> <p>925 combination defines the task completely. The <i>feasible activation</i></p> <p>926 <i>space</i> of the task, if it is well posed (37), is defined by the points \mathbf{a}</p> <p>927 that lie within the n-cube and at the intersection of all constraint</p> <p>928 hyperplanes.</p> <p>929 Geometrically speaking, the feasible activation space is a $(n-m)$-</p> <p>930 dimensional convex polytope P embedded in \mathbb{R}^n that contains all n-</p> <p>931 dimensional muscle coordination patterns (i.e., points \mathbf{a}) that satisfy</p> <p>932 all constraints, and therefore can produce the task. Increasing</p> <p>933 task specificity by adding more constraints naturally decreases</p> <p>934 the dimensionality and changes the size and shape of the feasible</p> <p>935 activation space (20, 30, 51).</p> <p>936</p> <p>The Hit-and-Run algorithm uniformly samples from feasible activa-</p> <p>tion spaces Calculating the geometric properties of convex poly-</p> <p>937 topes in high dimensions is computationally challenging. Taking</p> <p>938 the generalized concept of an n-dimensional volume as an example</p> <p>939 of a geometric property of interest, the exact volume computations</p> <p>940 for n-dimensional polytopes is known to be tractable only in a poly-</p> <p>941 nomial amount of time (i.e., $\#P$-hard) (52). Currently available</p> <p>942 volume algorithms can only handle polytopes embedded in small</p> <p>943 dimensions like 10 or slightly more (53). Studying vertebrate limbs</p> <p>944 in general, however, can require including several dozen muscles,</p> <p>945 such as our studies of a 17-muscle human arm and a 31-muscle cat</p> <p>946 hindlimb model (29); and other limb models have over 40 muscles</p> <p>947 such as (1, 54–56).</p> <p>948 Similar difficulties arise when computing other geometric proper-</p> <p>949 ties such as the shape and aspect ratio of P in high dimensions. We</p> <p>950 and others have described polytopes P by their bounding box (i.e.,</p> <p>951 the range of values in every dimension) (30, 33), but that singularly</p> <p>952 overestimates the shape and volume of the feasible activation space</p> <p>953 as discussed in (29). Take Fig. ??e as an example, where the bound-</p> <p>954 ing box of the 2-dimensional polygon has a volume—even though a</p> <p>955 plane has zero volume—, and can be almost as large as the positive</p> <p>956 unit cube itself. Similar problems arise in the interpretation of the</p> <p>957 inscribed and circumscribed ball (57).</p> <p>958 We applied the Hit-and-Run method to sample points from the</p> <p>959 feasible activation space—a method that is evaluated and justified in</p> <p>960 (18?). This complete probabilistic method describes the structure</p> <p>961 of feasible activation spaces P with a set of uniformly-at-random</p> <p>962 muscle activation patterns that produce the same wrench. This</p> <p>963 enables us to derive descriptive statistics, histograms, and point</p> <p>964 densities of the set of valid muscle activation patterns \mathbf{a} uniformly</p> <p>965 sampled from the polytope. To do so, we use the Hit-and-Run</p> <p>966 method. We have presented a detailed explanation of the theory</p> <p>967 (In Chapter X of (?)), have justified the utility of this method on</p> <p>968 tendon-driven models of the index finger (?).</p> <p>969</p> <p>Example of a tendon-driven system.</p> <p>970</p> <p>Realistic 3-D model of a 7-muscle human index finger We applied</p> <p>971 this methodology to our published model of an index finger for</p> <p>972 static fingertip force production. The model is described in detail</p> <p>973 elsewhere (58). Briefly, the input to the model is a 7-D muscle</p> <p>974 activation pattern \mathbf{a}, and the output is a 4-D wrench (i.e., static</p> <p>975 forces and torque) at the fingertip \mathbf{w}.</p> <p>976</p> $\mathbf{w} = H\mathbf{a} \quad [2]$ $H = J^{-T}RF_o \quad [3]$ $H \in \mathbb{R}^{4 \times 7} \quad [4]$ <p>977</p> <p>where</p> $\mathbf{a} = \begin{pmatrix} a_{FDP} \\ a_{FDS} \\ a_{EIP} \\ a_{EDC} \\ a_{LUM} \\ a_{DI} \\ a_{PI} \end{pmatrix} \quad [5]$ <p>978</p> <p>In Cartesian coordinates, the 4-D output wrench corresponds to</p> <p>979 the anatomical directions shown in Fig. 1e.</p> <p>980</p> $\mathbf{w} = \begin{pmatrix} f_x \\ f_y \\ f_z \\ \tau_x \end{pmatrix} = \begin{pmatrix} f_{radial} \\ f_{distal} \\ f_{palmar} \\ \tau_{radial} \end{pmatrix} \quad [6]$ <p>981</p> <p>The biomechanical model H includes three serial links articu-</p> <p>982 lated by four kinematic degrees of freedom (ad-abduction, flexion-</p> <p>983 extension at the metacarpophalangeal joint, and flexion-extension at</p> <p>984 the proximal and distal interphalangeal joints). The action of each</p> <p>985 of the seven muscles (FDP: <i>flexor digitorum profundus</i>, FDS: <i>flexor</i></p> <p>986 <i>digitorum superficialis</i>, EIP: <i>extensor indicis proprius</i>, EDC: <i>exten-</i></p> <p>987 <i>sor digitorum communis</i>, LUM: <i>lumbrical</i>, DI: <i>dorsal interosseous</i>,</p>
--

and PI: *palmar interosseous*) on each joint to produce torque is given by the moment arm matrix $R \in \mathbb{R}^{4 \times 7}$. Lastly, $J \in \mathbb{R}^{4 \times 4}$ and $F_0 \in \mathbb{R}^{7 \times 7}$ are the Jacobian of the fingertip with 4 kinematic degrees of freedom, and the diagonal matrix containing the maximal strengths of the seven muscles, respectively (18, 44). The finger posture was defined to be 0° ad-abduction and 45° flexion at the metacarpophalangeal joint, and 45° and 10° flexion, respectively, at the proximal and distal interphalangeal joints.

Feasible activation space for a static fingertip force task Our goal is to find the family of all feasible muscle activation patterns that can produce a given task. In particular, the task we explored is producing various magnitudes of a submaximal static force in the distal direction f_{distal} — in the absence of any τ_{radial} , shown in Fig. 1f. Therefore the feasible activation space is a polytope P in 7-dimensional activation space that meets the following four linear constraints in \mathbf{a} (18, 21, 44)

$$f_{radial} = 0 \quad [7]$$

$$f_{distal} = \text{desired magnitude as \% of maximal} \quad [8]$$

$$f_{palmar} = 0 \quad [9]$$

$$\tau_{palmar} = 0 \quad [10]$$

These four constraints on the static output of the finger yield a 3-dimensional (i.e., $7 - 4 = 3$) polytope P embedded in 7-dimensional activation space. For details on how to create such models, apply task constraints and find such polytopes via vertex enumeration methods, see (18).

For the index finger model used in this paper, the published maximal feasible force in the distal direction is 28.81 Newtons. We defined the normalized desired distal task intensity as a value ranging between 0 and 1, i.e., each submaximal force can be produced by any of the points contained in its corresponding feasible activation space. For the production of a maximal force with $\alpha = 1$ the feasible activation space shrinks to a single point (12, 19, 37, 44).

Analysis of feasible activation spaces.

Parallel coordinates visualization shows the location of all points across all dimensions Parallel coordinates are a common graphical approach to visualize interactions among high-dimensional data, which has been used in biomechanical studies (59, 60). To demonstrate this visualization method, consider the results of the simple 3-dimensional example shown in Fig. ??e. We begin by drawing n parallel vertical lines for each of the dimensions n (i.e., 3 muscles). With the axis limits of each line set between 0 and 1, each point (Fig. 2a) is then represented by connecting their coordinates by $n - 1$ lines as shown in Fig. 2b.

Neural and metabolic cost functions As mentioned in the Introduction, the field of neuromuscular control has a long historical tradition of using optimization to find muscle activation patterns that minimize effort, which requires the (often contentious) definition of cost functions (12, 13, 16, 19). Therefore, we used four representative cost functions to calculate the relative fitness of each of the muscle activation patterns sampled—in effect also calculating the fitness landscape across all possible solutions. The cost functions are defined at the level of neural effort (L_1 , and L_2 norms); and at the level of metabolic cost, thought to be approximated by neural drive weighted by the strength of each muscle (L_1^w and L_2^w norms) (13, 16).

To visualize the costs associated with each valid muscle coordination pattern, we simply added four vertical lines at the far right of the parallel coordinates plot, one for each cost function, Fig. 2c. The variables a_i and F_{0i} represent the activation of the i^{th} muscle in a given muscle activation pattern, and the maximal strength of each muscle (13, 16). Maximal muscle strengths are approximated by the multiplying each muscle's physiological cross-sectional area,

in cm^2 , by the maximal active muscle stress of mammalian muscle, 35 N/cm^2 (61). These four cost functions are but four examples as the literature contains many others as any investigator is in fact free to chose any cost function deemed relevant to their study.

Histograms of the activation level of each muscle across all valid solutions Muscle-by-muscle histograms are another straightforward way to visualize the many points sampled from the convex polytope. Histograms are particularly helpful because they are approximations to probability density functions. They visualize the relative number of solutions (i.e., density of solutions) that required a particular level of activation from a particular muscle within its range of $[0, 1]$. In addition, the upper and lower bounds of the histograms show, in fact, the size of the side of the bounding box of the polytope in every dimension (i.e., for independently controlled muscle).

Dimensionality reduction Investigators have repeatedly reported that electromyographical signals (i.e., experimental estimates of muscle activation patterns) tend to exhibit strong correlations with one another. In these experimental descriptions of dimensionality reduction of neuromuscular control, only few independent functions—sometimes called synergies—suffice to explain the majority of the variability in the observed muscle activation patterns (1–4, 6, 7, 62). Principal components analysis (PCA) is a widely used technique to extract these few independent basis functions (correlation vectors called principal components, PCs) from high-dimensional data (63). In this case, PCs are often called the experimental representations of synergies of neural origin (1).

Therefore, we also applied PCA to points (i.e., muscle coordination patterns) sampled from the feasible activation space at each force level. This provides the PCs that describe the correlations among valid muscle activation patterns for a given task. For example, the feasible activation space P in Fig. ??e is a 2-dimensional polygon embedded in 3-dimensional activation space. Thus, applying PCA to points sampled from the polygon will extract 2 synergies (i.e., 3-dimensional correlation vectors PC1 and PC2) that wholly explain the feasible activation space. By extension, in the case of fingertip force production in Fig. 1, the feasible activation space is a 3-dimensional polytope embedded of the 7-dimensional activation space. And PCA should extract, by construction, as many synergies as there are dimensions in the feasible activation space. For static force production with the index fingertip (i.e., 7 muscles and 4 constraints), we know that 3 principal components should describe 100% of the variance in points sampled from the feasible activation space (i.e., 7-dimensional correlation vectors PC1, PC2, and PC3).

Applying PCA to our data allows us to test whether and how its results change when applied to feasible activation spaces for different magnitudes of fingertip force. We applied PCA to feasible activation spaces for fingertip task intensities ranging from 0 to 90% of maximal. We compare both the variance explained by each PC and their vector direction (i.e., the ‘loadings’ or correlations among muscle (64)) as the force level increases. Lastly, we tested whether our PCA results are sensitive to the number of points sampled from each feasible activation space. This is important because experimental studies test 10 or so subjects in practice, which may be too few when sampling from high-dimensional spaces.

ACKNOWLEDGMENTS. Research reported in this publication was supported by the National Institute of Arthritis and Musculoskeletal and Skin Diseases of the National Institutes of Health (NIH) under Awards Number R01 AR-050520 and R01 AR-052345 to FVC, and the Swiss National Science Foundation (SNF Project 200021_150055 / 1) to BG, KF and FVC. The content is solely the responsibility of the authors and does not necessarily represent the official views of the SNSF or the NIH. We thank Komei Fukuda for his integral support in designing this research collaboration. We thank J Pugliesi, T Kim, C Lim, A Baugus, P Vachhani, and A Boling for extending the scientific rigor of this work through reviews, documentation, and code

- Kutch J, Valero-Cuevas F (2012) Challenges and new approaches to proving the existence of muscle synergies of neural origin. *PLoS Computational Biology* 8(5):e1002434.
- Steele KM, Tresch MC, Perreault EJ (2013) The number and choice of muscles impact the results of muscle synergy analyses. *Frontiers in computational neuroscience* 7.
- Bizzi E, Cheung VC (2013) The neural origin of muscle synergies. *Frontiers in computational neuroscience* 7.
- Dingwell JB, John J, Cusumano JP (2010) Do humans optimally exploit redundancy to control step variability in walking? *PLoS computational biology* 6(7):e1000856.
- Rácz K, Valero-Cuevas FJ (2013) Spatio-temporal analysis reveals active control of both task-relevant and task-irrelevant variables. *Frontiers in computational neuroscience* 7.
- Steele KM, Tresch MC, Perreault EJ (2015) Consequences of biomechanically constrained tasks in the design and interpretation of synergy analyses. *Journal of neurophysiology* 113(12):1296–1308.
- Łovász L (1999) Hit-and-run mixes fast. *Mathematical Programming* 86(3):443–461.
- Kutch JJ, Valero-Cuevas FJ (2011) Muscle redundancy does not imply robustness to muscle dysfunction. *Journal of Biomechanics* 44(7):1264–1270.
- Valero-Cuevas FJ (2000) Predictive modulation of muscle coordination pattern magnitude scales fingertip force magnitude over the voluntary range. *J. Neurophysiol.* 83:1469–1479.
- De Rugy A, Loeb GE, Carroll TJ (2012) Muscle coordination is habitual rather than optimal. *The Journal of Neuroscience* 32(21):7384–7391.
- Loeb G (2012) Optimal is not good enough. *Biological Cybernetics* 106(1–12):757–765.
- Chvatal V (1983) *Linear programming*. (Macmillan).
- Smith RL (1984) Efficient monte carlo procedures for generating points uniformly distributed over bounded regions. *Operations Research* 32(6):1296–1308.
- Łovász L (1999) Hit-and-run mixes fast. *Mathematical Programming* 86(3):443–461.

biomechanics 33(12):1601–1609.

33. Kutch JJ, Valero-Cuevas FJ (2011) Muscle redundancy does not imply robustness to muscle dysfunction. *Journal of Biomechanics* 44(7):1264–1270.

34. Valero-Cuevas FJ (2000) Predictive modulation of muscle coordination pattern magnitude scales fingertip force magnitude over the voluntary range. *J. Neurophysiol.* 83:1469–1479.

35. De Rugy A, Loeb GE, Carroll TJ (2012) Muscle coordination is habitual rather than optimal. *The Journal of Neuroscience* 32(21):7384–7391.

36. Loeb G (2012) Optimal is not good enough. *Biological Cybernetics* 106(1–12):757–765.

37. Chvatal V (1983) *Linear programming*. (Macmillan).

38. Smith RL (1984) Efficient monte carlo procedures for generating points uniformly distributed over bounded regions. *Operations Research* 32(6):1296–1308.

39. Łovász L (1999) Hit-and-run mixes fast. *Mathematical Programming* 86(3):443–461.